


## Article

# Influence of Continuous Provision of Synthetic Inertia on the Mechanical Loads of a Wind Turbine

Arne Gloe <sup>1,\*</sup>, Clemens Jauch <sup>1</sup> , Bogdan Craciun <sup>2</sup>, Arvid Zanter <sup>3</sup> and Jörg Winkelmann <sup>2</sup>

<sup>1</sup> Wind Energy Technology Institute, Flensburg University of Applied Sciences, 24943 Flensburg, Germany; clemens.jauch@hs-flensburg.de

<sup>2</sup> Innovation and Strategic Research, SUZLON Energy Ltd., 18057 Rostock, Germany; bogdan.craciun@suzlon.com (B.C.); joerg.winkelmann@suzlon.com (J.W.)

<sup>3</sup> Key Components, SUZLON Energy Ltd., 18057 Rostock, Germany; arvid.zanter@suzlon.com

\* Correspondence: arne.gloe@hs-flensburg.de

**Abstract:** In many electrical grids, the share of renewable energy generation increases. As these generators are typically connected to the grid via inverters, the level of grid inertia decreases. Such grids may therefore suffer from high rates of change of frequency during power imbalances. Modern wind turbines can help in controlling the frequency in such grids by providing synthetic inertia. A controller to provide synthetic inertia with wind turbines was developed at the Wind Energy Technology Institute in collaboration with Suzlon Energy. For this controller the influence of providing synthetic inertia on the mechanical loads of the wind turbine is assessed for different grid frequency scenarios. Such a scenario-based load analysis has not been published before, especially as the scenarios are derived from real measurements. The effect of the loads strongly depends on the analyzed grid frequency behavior. Ten months of high quality grid frequency measurements of the Indian grid are analyzed in order to derive inputs for the load calculation. Different types of grid frequency abnormalities are identified and categorized with respect to their severity. Based on the observed occurrences of the grid frequency abnormalities, realistic scenarios for the load calculations are chosen. The load calculations are performed for a state-of-the-art Suzlon wind turbine generator. The load increases caused by the supply of synthetic inertia are calculated for individual components assuming an otherwise undisturbed power production of the wind turbine in turbulent wind. Furthermore, a hardware-in-the-loop test bench is used to show how the measured grid frequencies are actually perceived by the control system of a typical wind turbine. The original frequency data were recorded with high quality measurement equipment, which is faster and more accurate than a multi-function relay, often used in wind turbines. For exemplary time traces, the effect of the reduced measurement accuracy on the reaction of the wind turbine is shown. This aspect has not been investigated in the literature yet. The results show that wind turbines can provide synthetic inertia without a considerable effect on the lifetime of the wind turbine. However, there are still problems with providing synthetic inertia reliably at high power operating points, which have to be solved.

**Keywords:** frequency support; grid frequency analysis; mechanical loads; rate of change of frequency; synthetic inertia; wind turbine; wind turbine generator



**Citation:** Gloe, A.; Jauch, C.; Craciun, B.; Zanter, A.; Winkelmann, J. Influence of Continuous Provision of Synthetic Inertia on the Mechanical Loads of a Wind Turbine. *Energies* **2021**, *14*, 5185. <https://doi.org/10.3390/en14165185>

Academic Editors: Adrian Ilinca and Davide Astolfi

Received: 5 July 2021

Accepted: 20 August 2021

Published: 22 August 2021

**Publisher's Note:** MDPI stays neutral with regard to jurisdictional claims in published maps and institutional affiliations.



**Copyright:** © 2021 by the authors. Licensee MDPI, Basel, Switzerland. This article is an open access article distributed under the terms and conditions of the Creative Commons Attribution (CC BY) license (<https://creativecommons.org/licenses/by/4.0/>).

## 1. Introduction

Modern power systems with high shares of inverter-based renewables are bound to exhibit little system inertia. In order to avoid unfavorable excursions of the grid frequency, and high rates of change of frequency (RoCoFs), system operators increasingly require the provision of grid frequency support from renewables. Such grid support is mandatory for instance in Ireland [1], Québec [2] and India [3]. The existing requirements are typically tailored to the system operator's specific needs and their individual control objectives. It has been shown for various countries that such demands can make future power systems

with high degrees of non-synchronous penetration more stable, e.g., in Ireland [4], the UK [5] and South Africa [6]. There are various strategies to support the grid frequency with wind turbine generators (WTGs) [7]. The frequency support is typically categorized in fast frequency response (a fast reacting frequency support service, which activates power proportionally to the grid frequency deviation—this is comparable to traditional primary frequency control) and the provision of synthetic inertia (reacting proportionally to the derivative of the frequency) [8]. In addition, there are various control schemes tailored to the needs of a specific grid operator, e.g., providing a predefined power increase for approximately ten seconds, if a frequency threshold is violated [9]. The provision of synthetic inertia with WTGs was first proposed in 2007 by Ramtharan et al. [10]. In this paper, the effect of continuous provision of synthetic inertia (SI) with the so-called variable H controller [11] is researched, which improves the state-of-the-art concepts by considering the current operating point of the WTG. In comparison to an event-based activation of SI, continuous provision of SI stabilizes the grid also during smaller power imbalances in the grid. Hence, it may help stabilizing the frequency in future grids with little inertia.

Traditionally, WTG control aims to maximize the energy yield of the WTG while keeping the resulting structural loads at an acceptable level [12]. The main sources of WTG loads (aerodynamic, inertial and gravitational [13]) have traditionally been addressed by using a PI(D)-controller with gain scheduling for the speed and power control of the WTG [14]. Additionally, the drive train and the tower of the WTG are often protected by a drive train and tower damper, which modifies the power setpoint of the WTG to reduce the loads on these components [15]. More recent developments in WTG control use state estimation and sensor fusion [16,17], as well as self-learning algorithms [18,19], to improve the WTG control and to make it more robust. In addition to these purely control-based improvements, control concepts which require additional hardware have lately been proposed, e.g., Lidar-based systems [20], tuned-mass dampers in the tower [21] or a tunable flywheel in the rotor of the WTG [22]. Structural loads resulting from the electrical grid are traditionally limited to grid faults, e.g., a low-voltage ride through events, which result in high mechanical stress for the drive train [23,24]. Suzlon has been researching this topic for many years already [25]. During such events, the main goal is to protect the WTG while keeping it connected to the grid. By contrast, grid frequency support mainly aims to stabilize the frequency of the electrical grid. The control system of the WTG must therefore handle the dynamic excitation from the wind and, in addition, the dynamic excitation from the grid. These excitations from the grid must be quantified and might have to be considered in the load calculation of a WTG comparably to the excitations from the wind. While the effect of frequency support on the grid is well studied, there is little research on the consequences for the mechanical loads of the supporting WTGs. Fleming et al. [26] compared different derating strategies of the WTG for fast frequency control and calculated the effect on the WTG loads. The authors did not use specific frequency scenarios but assumed that the WTG remains in derated operation during its entire lifetime. Wang et al. [27] did a similar study for different synthetic inertia control methods, which were tested for two predefined frequency scenarios at two different wind speeds. Fischer et al. recently published a comprehensive report [28] on the interactions between the supply of various grid services and structural loading of the WTG, e.g., the effect of SI provision on the drive train [29]. However, there is a lack of publications, which combine scenarios based on real data (i.e., with a defined severity and frequency of occurrence) with a comprehensive load analysis. This is problematic, as the results of the load analysis largely depend on the analyzed scenarios. This paper aims to close this research gap by analyzing high quality data of the Indian grid frequency and defining scenarios for the load calculation from this analysis. A load calculation for a state-of-the-art Suzlon DFIG WTG is performed, which shows the effect of continuous provision of SI with the variable H controller in the defined scenarios. Furthermore, hardware-in-the-loop (HiL) tests are carried out, which show the grid frequency actually perceived by the WTG when an industry standard measurement system is used. In fact, the work presented

in the paper closes a critical gap in the development of wind turbines. Wind turbine manufacturers have to be able to assess the lifetime consumption, resulting from newly demanded services and excitations. Therefore, the presented analytical approach is chosen to quantify the excitations from the grid frequency. In this context, it is important to note that the grid frequency does not behave as stochastic as the wind. However, it does not behave deterministically either. Hence, there are three aspects which define the novelty of the paper: (I) simulation of comprehensive scenarios based on real grid frequency measurements for (II) a state-of-the-art WTG (III) considering the real measurement system of the WTG.

The rest of the paper is structured as follows: Section 2 of this paper describes the used frequency data set and the method to derive load simulation scenarios from it. Furthermore, the HiL setup and the simulation environment for the load calculations is outlined. Section 3 presents and discusses the results of the scenario definition, the hardware-in-the-loop test and the load calculations. Section 4 summarizes the findings.

## 2. Methodology, Measurement Setup, Data Analysis and Simulation Model

The methodology used in this paper is summarized in Figure 1. Scenarios for the load calculations are derived from high-quality recordings of the Indian grid frequency. These scenarios are tested for different wind conditions and controller settings in a Flex5 [30] WTG model. Based on these time domain results, the effect of frequency support on the WTG loads are calculated for the design load case 1.2 [31]. Furthermore, a representative subset of the frequency scenarios is tested in a HiL setup. These six modified time traces are also tested in the Flex5 model. The WTG reaction to the six HiL and the corresponding original scenarios are compared by analyzing accelerations of the most vulnerable WTG components. This allows estimating the effect of the real measurement system in the WTG on the controller-induced loads.

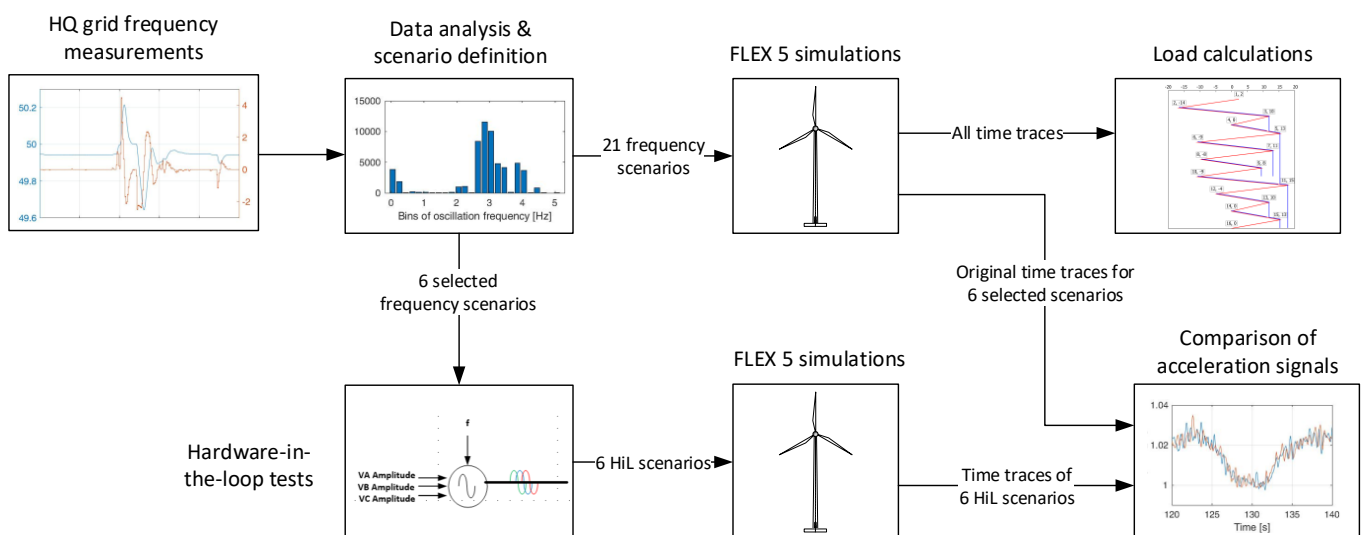


**Figure 1.** Overview of the used methodology.

After briefly introducing the variable H controller concept, the remainder of this section is structured along the three aspects of the load calculation: scenario definition, HiL tests and load simulation environment.

### 2.1. Variable H Controller

As this paper deals with the consequences of using the variable H controller, the concept of this controller is briefly introduced. The basic idea of the controller is that the grid operator defines an inertia constant ( $H_{dem}$ ). The WTGs emulate the inertial response (IR) of a synchronous generator with the defined inertia constant, when the WTGs operate

at a rated speed (see Equations (1) and (2); [32]). However, unlike synchronous generators, the rotational speed of a WTG changes with its operating point. Therefore, the variable inertia constant scales with the operating point of the WTG in accordance with the available kinetic energy stored in its rotation (see Equation (2)). Hence, the WTG provides as much IR as possible in its current operating point, while minimizing the risk of reducing the WTG speed too much.

$$P_{SI} = -2 \cdot H_{var} \cdot P_{rated} \cdot \frac{RoCoF}{f_{grid}} \quad (1)$$

where  $P_{SI}$  is the power change for SI,  $P_{rated}$  is the rated power of the WTG and  $H_{var}$  is the variable inertia constant.

$$H_{var} = H_{dem} \cdot \frac{0.5 \cdot J_{WT} \cdot (\omega_{gen}^2 - \omega_{cut-in}^2)}{0.5 \cdot J_{WT} \cdot (\omega_{rated}^2 - \omega_{cut-in}^2)} \quad (2)$$

where  $H_{dem}$  is the inertia constant to be emulated as defined by the grid operator,  $\omega_{gen}$  is the generator speed,  $\omega_{cut-in}$  is the generator speed at which the WTG starts to produce power and  $\omega_{rated}$  is the rated generator speed of the WTG.

The power controller of the WTG is modified by adding  $P_{SI}$  to the optimal power derived from the power-vs-speed characteristic of the WTG (see Figure 2). Therefore,  $P_{SI}$  directly influences the power reference of the WTG power controller and grid frequency abnormalities may directly affect the WTG dynamics. Please note that, for the sake of clarity, Figure 2 does not show an additional controller mentioned in the introduction (e.g., drive train damper).

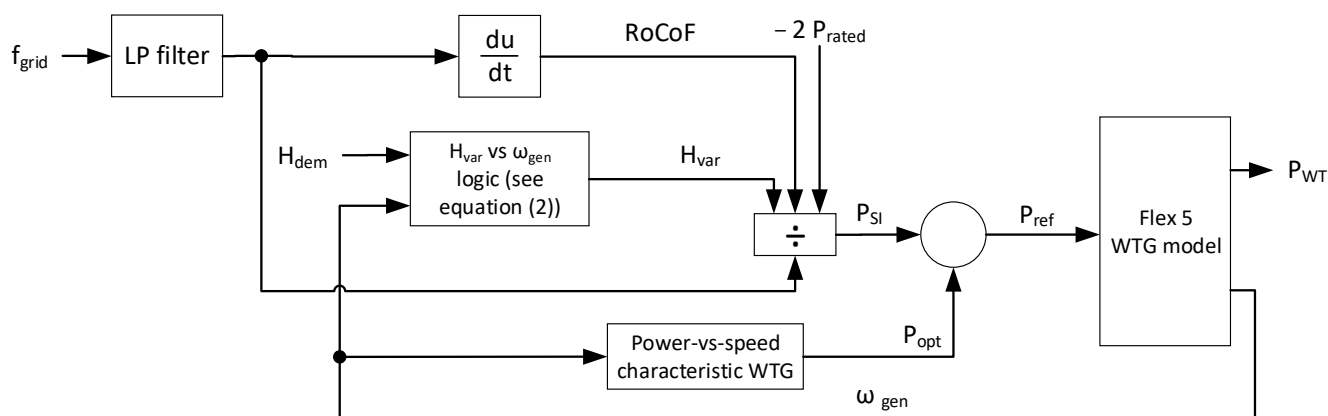


**Figure 2.** Power setpoint calculation and interaction with the WTG Flex5 model.

## 2.2. Grid Frequency Analysis and Scenario Definition

For the scenario definition, frequency measurements from the Western Indian power system are analyzed. The data were recorded between March 2015 and January 2016 following the then most recent IEC 61,400 standard [33] with a state-of-the-art measurement system and a sample time of 20 ms (in total 1,025,220,000 samples, equivalent to 237.3 days of uninterrupted measurements). The accuracy of the measurement system is 0.9 mHz. Hence, the smallest recognizable RoCoF is 0.045 Hz/s.

Load calculations in a previous project [34] showed that the effect of SI provision on WTG loads during normal frequency behavior is negligible. Therefore, the analysis focuses on two different abnormalities of the grid frequency, which are identified in the dataset:

1. Grid frequency oscillations: defined as periodic variations of the grid frequency. Oscillations are identified by a violation of a frequency-dependent amplitude thresholds in the frequency domain.
2. Events: defined as abrupt changes of the grid frequency. Events are identified by a violation of the threshold for the RoCoF ( $|RoCoF| > 1$  Hz/s).

Both abnormalities were also analyzed in the previous project. However, a regular pattern in frequency events was not addressed, which leads to a very high number of events (>25,000/year) and eventually to questionable results of the load calculation. The previous study also did not account for different amplitudes and frequencies of grid frequency oscillations as it was only used one scenario for this abnormality. Hence, in this study the recorded grid frequency measurements are analyzed in detail in order to derive detailed scenarios that are more realistic.

The times during which grid frequency oscillations occur are identified with the help of an analysis in the frequency domain. For that purpose, an amplitude threshold in the frequency domain is defined, which leads to a power setpoint variation ( $P_{SI}/P_{rated}$ ) with an amplitude of at least 0.01 pu. To derive this threshold, Equation (1) can be solved for the minimum RoCoF leading to such a power variation using  $f_{grid,0} = 50$  Hz and  $H_{var} = H_{dem} = 6$  s [32]:

$$RoCoF_{min} = \frac{P_{SI}}{P_{rated}} \cdot \frac{f_{grid,0}}{-2 \cdot H_{var}} \quad (3)$$

The minimum RoCoF according to Equation (3) must be reached during a grid frequency oscillation. The general equation of a grid frequency oscillation (4) is used to derive the relation between the RoCoF and the amplitude and the frequency of the oscillation:

$$f_{grid}(t) = f_{grid,0} + A_{osc} \cdot \sin(2 \cdot \pi \cdot f_{osc} \cdot t) \quad (4)$$

where  $f_{grid}(t)$  is the instantaneous grid frequency,  $f_{grid,0}$  the center value of the grid frequency oscillation,  $A_{osc}$  the oscillation amplitude and  $f_{osc}$  the oscillation frequency.

Equation (4) can be derived with respect to time to calculate the RoCoF during the oscillation,  $RoCoF_{osc}$ :

$$RoCoF_{osc}(t) = A_{osc} \cdot 2 \cdot \pi \cdot f_{osc} \cdot \cos(2 \cdot \pi \cdot f_{osc} \cdot t) \quad (5)$$

The maximum RoCoF according to Equation (5) occurs when the cosine term is 1. Hence, Equation (5) can be simplified and solved for the amplitude of the grid frequency oscillation:

$$A_{osc} = \frac{RoCoF_{osc,max}}{2 \cdot \pi \cdot f_{osc}} \quad (6)$$

In order to derive the amplitude threshold in the frequency domain, the maximum RoCoF during the oscillation,  $RoCoF_{osc,max}$ , in Equation (6), is substituted by the minimum RoCoF according to Equation (3). Hence, the modified Equation (6) can be used as amplitude threshold in the frequency domain.

In order to find times with relevant grid frequency oscillations, the recorded grid frequency measurements are split into overlapping intervals (see Figure 3). The Fourier transform of each interval is compared to the amplitude threshold according to Equations (3) and (6). Intervals, for which a relevant oscillation is detected, are marked in green in Figure 3, while the others are marked in red. Whenever frequency oscillations in adjacent intervals are detected, these intervals are combined in a single time trace. For the example given in Figure 3, intervals 3 to 6 (and all further intervals until the end of the ongoing oscillation) are combined into a single time trace containing the full duration of the oscillation.

In order to define a reasonable number of scenarios for the load calculation, the detected time traces of grid frequency oscillations are binned with respect to the oscillation frequency. It is assumed that grid frequency oscillations with an oscillation frequency close to the eigenfrequency ( $f_{eigen}$ ) of WTG components are more harmful to the respective component (due to resonance effects). Therefore, narrow frequency bins ( $f_{eigen} \pm 10\%$ ) are used around the most important eigenfrequencies of the WTG. All other oscillations of the grid frequency are grouped and analyzed in three wider bins (see below). For the load analysis, the scenarios must be properly defined in terms of typical RoCoFs during the oscillation and the duration of the oscillation:

1. RoCoF during oscillation: The changes of the power setpoint for SI is directly proportional to the occurring RoCoF (see Equation (1)). Hence, a representative RoCoF has



to be defined for each oscillation bin. For this purpose, the weighted average of the RMS value of the RoCoF of all time traces in a bin is calculated. The duration of the individual time traces is used as a weighting factor. Longer time traces have therefore more influence on the average RoCoF than shorter time traces. The results are chosen as the representative RoCoF for the corresponding frequency bins.

2. Duration of oscillation: A longer grid frequency oscillation may be more harmful to the WTG than a shorter one, especially when resonance may occur. Hence, a representative duration has to be defined for each frequency bin. For this purpose, the weighted average duration is calculated for each frequency bin. The RoCoF of the individual time traces is used as a weighting factor, as stronger oscillations are more harmful to the WTG than weaker ones. The resulting durations are chosen as the representative duration for the corresponding frequency bins.

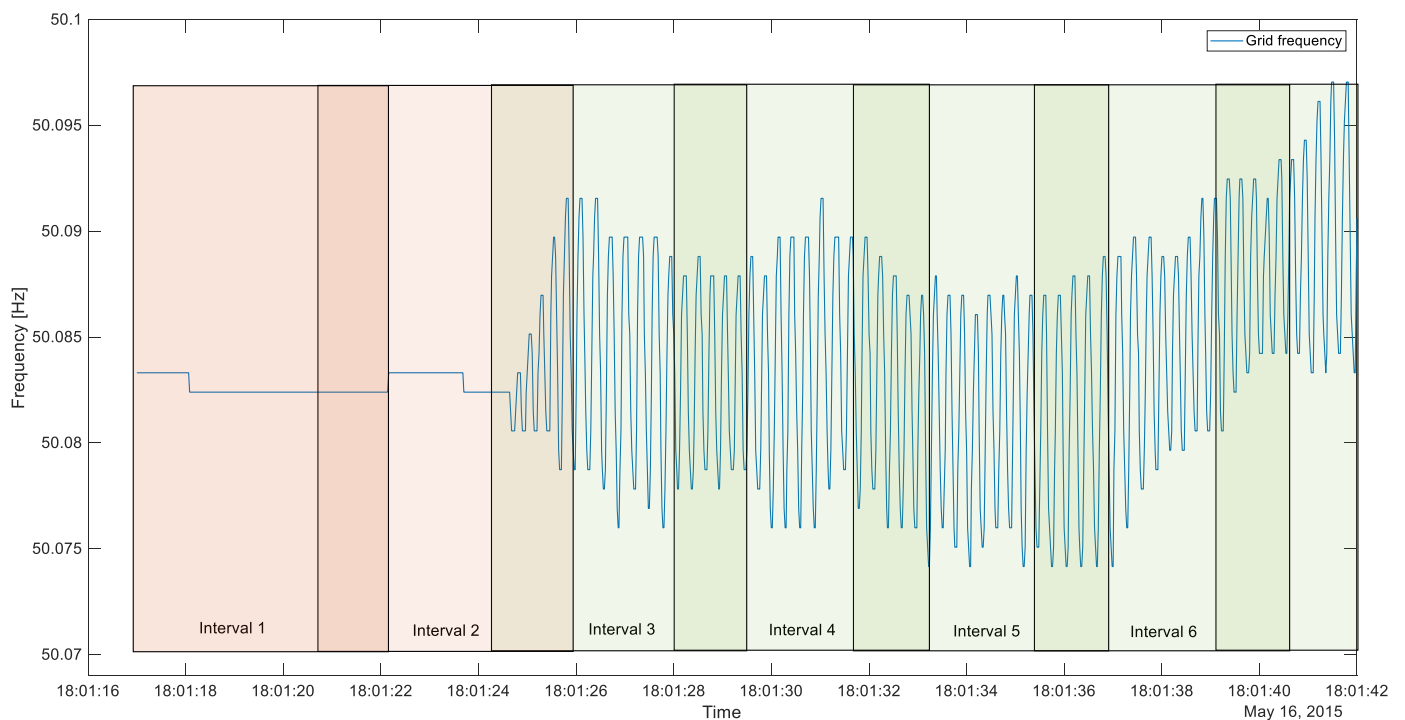


**Figure 3.** Example of a beginning grid frequency oscillation and the detection intervals. Red-shaded boxes mark intervals in which no oscillation is detected, while green-shaded boxes mark intervals with oscillations.

The analysis showed that the majority of the grid frequency oscillations occurred with an oscillation frequency between 2.6 Hz and 4.6 Hz (see Figure 4). Furthermore, there is a second cluster with an oscillation frequency below 0.4 Hz. The lack of oscillations with a frequency between 0.4 Hz and 2.6 Hz is actually beneficial, as most eigenfrequencies of the vulnerable components of the considered WTG are within this frequency range. Hence, scenarios for WTG components only have to be defined for the 1st eigenfrequency of the tower and for the 2nd bending eigenfrequency of the blades (see Table 1). It has to be noted that the eigenfrequencies of the relevant component may differ depending on the WTG design, which would influence the choice of scenarios. For this particular WTG, five scenarios are defined which represent grid frequency oscillations in the load analysis (see Table 1). In addition to the three properties described above, the total duration of the time traces in each oscillation bin is given in Table 1 and is used as a likelihood of occurrence (i.e., % of measurements in which such oscillations occur). The time traces for the scenarios were chosen such that the representative RMS value of the RoCoF and the representative duration as defined above are met.

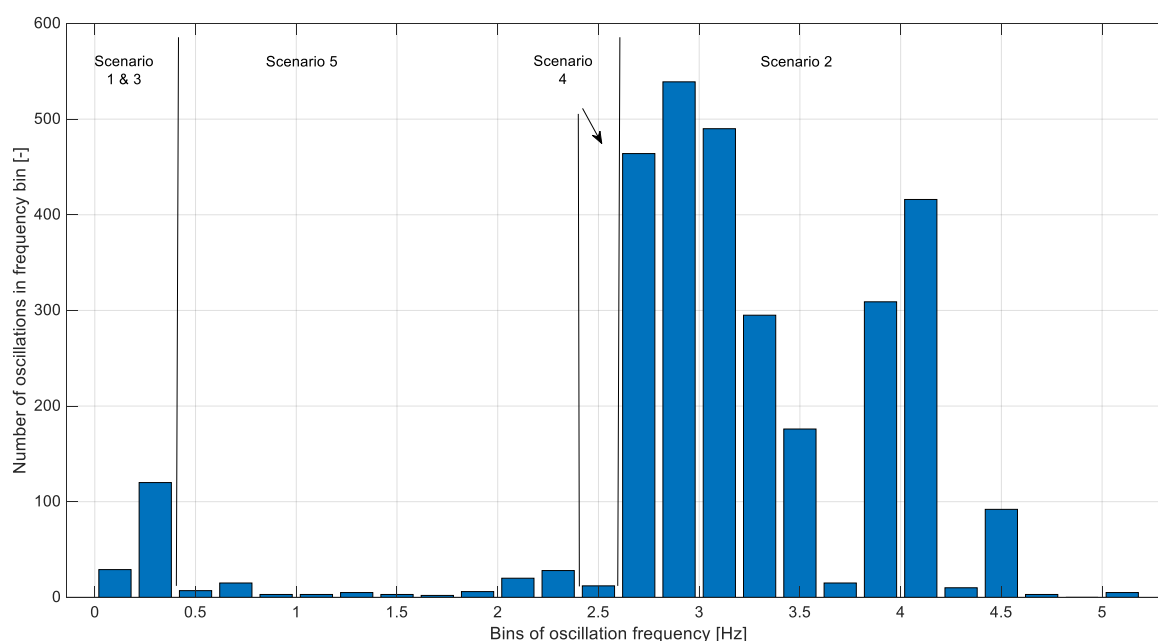


**Figure 4.** Number of detected periods with grid frequency oscillation with respect to the binned oscillation frequency (bin width 0.2 Hz). Number of the scenario, which represents the accumulated oscillations.

**Table 1.** Overview of identified scenarios to represent grid frequency oscillation in the load analysis.

Scenario Number	Oscillation Frequency	RoCoF <sub>RMS</sub>	Duration	Likelihood of Occurrence	Comment for Scenario
1	0.26 Hz	0.1 Hz/s	77 s	0.007%	Low frequency oscillation
2	2.73 Hz	0.09 Hz/s	20 s	0.21%	High frequency oscillation
3	0.3 Hz	0.07 Hz/s	22 s	0.004%	Tower 1st eigenfrequency
4	2.4 Hz	0.127 Hz/s	61.7 s	0.008%	Blade 2nd bending eigenfrequency
5	2–2.3 Hz <sup>1</sup>	0.103 Hz/s	24 s	0.004%	Oscillations with a frequency between scenario numbers 3 and 4

<sup>1</sup> The dominant frequency changes during the oscillation period.

The second abnormality considered in this analysis are frequency events. Figure 5 shows an example of a frequency event, which occurred during the measurement campaign. The grid frequency increases temporarily to 50.2 Hz before dropping to 49.65 Hz within 500 ms and immediately returning to 49.95 Hz. The RoCoF threshold ( $\pm 1$  Hz/s) is violated several times during the event, both in a negative and a positive direction.

Events can be detected in the recorded grid frequency measurements by a violation of the RoCoF threshold. The properties of the detected events are analyzed in order to derive scenarios for the load calculation. For this purpose, the events are categorized based on three criteria:

1. Event type: An event occurs every twenty minutes in the recorded grid frequency measurements. The exact reason for these regular events is unknown, but it is likely caused by the measurement setup and is called an expected event. All other events are called unexpected events (e.g., see Figure 5). While the expected events may be avoided with a different measurement system, the other events are likely to be measured with any kind of system. For this study, only the unexpected events are considered in the load calculation.
2. Duration: During most events, the RoCoF threshold is violated several times during a short period, typically less than 500 ms. These events are called singular events,

e.g., a steep drop of the grid frequency followed by an immediate return to the steady state value. Sometimes, multiple singular events occur with very short pauses (e.g., see Figure 5) causing multiple excitations of the WTG before the WTG can return to its steady state operating point. Such multiple excitations are potentially more harmful for the WTG. Hence, such multiple events are considered separately in the load analysis. The event shown in Figure 5 is classified as a long event as the RoCoF threshold is violated several times between 13:06:05 and 13:06:06 and again at 13:06:07.5.

3. Maximum and minimum RoCoF: It is assumed that extreme RoCoFs are more harmful for the WTG. A combination of maximum and the minimum RoCoF is used to categorize individual events into clusters (see Figure 6).

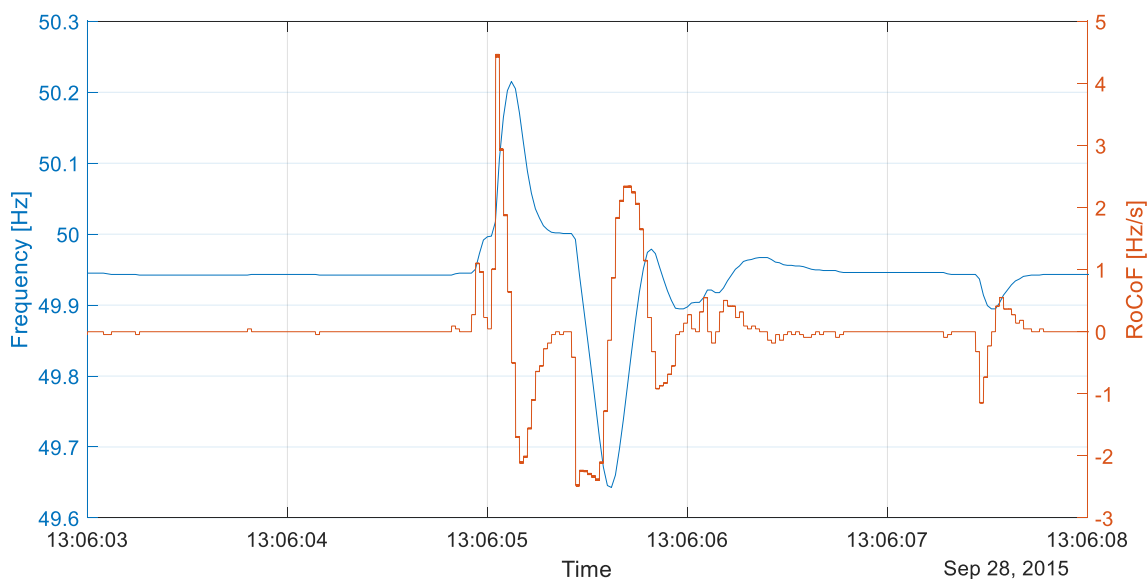
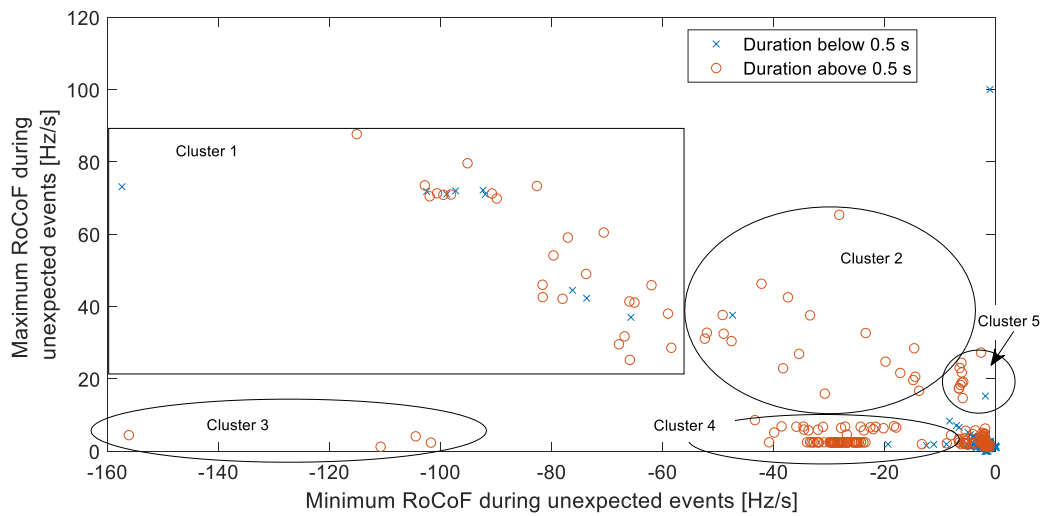


**Figure 5.** Example for an event of the grid frequency during which the RoCoF threshold is violated several times in a short period.

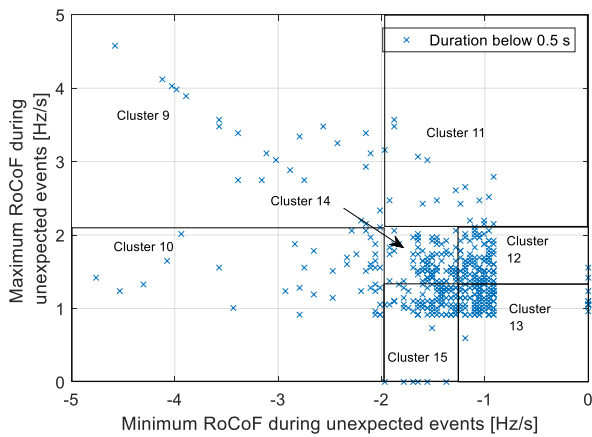
There were 2131 unexpected events detected in the analyzed data. These events are clustered with respect to the maximum and minimum RoCoF for two different durations (see Figure 6a–c). During 6.5% of the events extreme RoCoFs occurred (see Figure 6a) for which the detected grid frequency changed by up to  $-158$  Hz/s and  $+90$  Hz/s. These events were assigned to five clusters (see Figure 6a). The majority of the events showed smaller RoCoFs up to  $\pm 5$  Hz/s for short events and up to  $\pm 10$  Hz/s for long events. These events were grouped in detailed clusters: three clusters for long events (see Figure 6c) and seven cluster for short events (see Figure 6b). Even though the RoCoFs for these events are small in comparison to the extreme events in the data set, they still have a drastic effect on the power setpoint of a WTG providing SI.

For each cluster, a representative time trace of the grid frequency is chosen as a scenario for the load calculations (see Table 2). The only exception is cluster one, for which two separate time traces are chosen as the cluster contains many short and many long events. The number of detected events in the recorded grid frequency measurements is used to derive the expected number of events per year for each cluster. Data equivalent to 237.3 days of uninterrupted measurements are recorded, hence the scaling factor to 365 days is 1.54. As the measurement campaign only recorded data between March 2015 and January 2016, the data are also checked for seasonality effects, e.g., they are caused by the Indian monsoon. For the data at hand, no such effects stand out: grid frequency oscillations and events occurred with a similar likelihood throughout the months. Hence, a linear scaling seems appropriate.

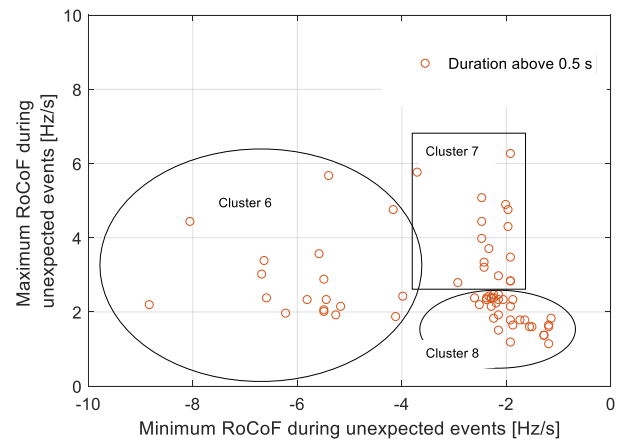




(a)



(b)



(c)

**Figure 6.** Cluster of grid frequency events depending on the maximum and minimum occurring RoCoFs and the event duration. (a) Short and long event for very high RoCoFs. (b) Short events for smaller RoCoFs. (c) Long events for smaller RoCoFs. (b,c) are an excerpt from (a) giving a detailed view of events with less extreme RoCoFs.

**Table 2.** Overview of identified event scenarios for the load analysis.

Scenario Number	Cluster	Upper Limit Minimum RoCoF	Lower Limit Minimum RoCoF	Lower Limit Maximum RoCoF	Upper Limit Maximum RoCoF	Duration	Number of Events in Dataset	Number of Events Per Year
6	1	-50 Hz/s	-120 Hz/s	25 Hz/s	90 Hz/s	long	27	42
7	1	-50 Hz/s	-120 Hz/s	25 Hz/s	90 Hz/s	short	9	14
8	2	-10 Hz/s	-50 Hz/s	15 Hz/s	75 Hz/s	long	19	29
9	3	-100 Hz/s	-160 Hz/s	0 Hz/s	20 Hz/s	long	4	6
10	4	-10 Hz/s	-50 Hz/s	0 Hz/s	15 Hz/s	long	77	118
11	5	0 Hz/s	-10 Hz/s	10 Hz/s	50 Hz/s	long	10	15
12	6	-4 Hz/s	-10 Hz/s	0 Hz/s	6 Hz/s	long	17	26
13	7	0 Hz/s	-4 Hz/s	2.5 Hz/s	10 Hz/s	long	16	25
14	8	0 Hz/s	-4 Hz/s	0 Hz/s	2.5 Hz/s	long	33	51
15	9	-2 Hz/s	-5 Hz/s	2 Hz/s	5 Hz/s	short	27	42
16	10	-2 Hz/s	-5 Hz/s	0 Hz/s	2 Hz/s	short	74	114
17	11	0 Hz/s	-2 Hz/s	2 Hz/s	5 Hz/s	short	41	63
18	12	0 Hz/s	-1.25 Hz/s	1.25 Hz/s	2 Hz/s	short	129	198
19	13	0 Hz/s	-1.25 Hz/s	0 Hz/s	1.25 Hz/s	short	548	843
20	14	-1.25 Hz/s	-2 Hz/s	1.25 Hz/s	2 Hz/s	short	108	166
21	15	-1.25 Hz/s	-2 Hz/s	0 Hz/s	1.25 Hz/s	short	244	375

The defined grid frequency scenarios are used in HiL tests and a Flex 5 simulation. Both setups are introduced in the following sections.

### 2.3. Hardware-in-the-Loop Tests Experimental Setup

The analyzed time traces of the grid frequency were measured with a high-quality measurement system, which is not available in a standard WTG. Hence, the WTG will measure a different frequency in an identical grid situation. In order to reduce the uncertainty, which arises from the different measurement systems, HiL tests of exemplary time traces are conducted (for scenarios 1, 2, 4, 7, 8 and 10). As the chosen time traces include typical characteristics of the time traces of all scenarios, the HiL tests are representative for all cases. For the HiL tests, the measured frequency signal is converted into three analogue AC voltage signals using a Typhoon HIL 602 [35], which are then measured by the original multi-function relay (MFR) of the WTG and processed in the original Bachmann [36] controller hardware (see Figure 7). The sample rate of the analogue inputs and outputs of the Bachmann controller is 1 ms. The frequency signal is sent to the Typhoon using an analog signal with the same sample rate. The Typhoon HIL 602 has a 1  $\mu$ s simulation time step and the analogue output is updated with the same rate. The sampling of the Typhoon HIL 602 can go down even to 20 ns. The MFR measures the grid frequency every 10 ms and submits its measurements to the Bachmann controller via a CAN connection.

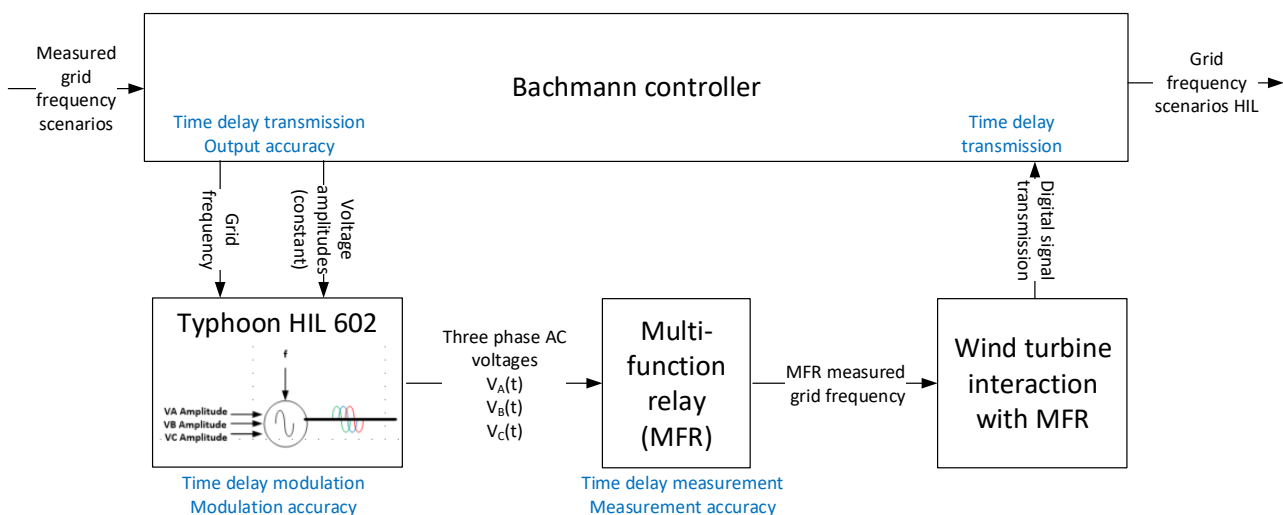


**Figure 7.** Measurement setup of the HiL tests and indication of the occurring accuracy issues and time delays.

However, these HiL tests can only reduce the uncertainty as it is inherently assumed that the grid frequency was measured perfectly. Furthermore, the output signal of the Bachmann controller has a limited accuracy and the created voltage signals are near perfect sinusoidal curves with a limited modulation accuracy. By contrast, the transmission of the MFR signal to the Bachmann controller does not limit the accuracy of the measured signal. The results of frequencies measured in the HiL tests are presented and discussed in Section 3.1. The resulting time traces are used in the FLEX 5 simulations (described in the following section) and are compared to the frequency time traces measured by the high-quality system to check whether the WTG reaction is affected by the limitation of its measurement system.

### 2.4. Wind Turbine Simulation Model and Load Calculations

The load calculations are based on time domain simulations of a novel DFIG WTG of the 3.x MW class, which will be introduced into the market in the near future. Due to the novelty of this WTG, the technical details, which may be published, are limited. The simulations are conducted with a Flex5 [30] model for the mechanical part of the

WTG. The model has 20 degrees of freedom (4 for each blade, 2 for the main shaft, 6 for the tower). A second order model of the generator-converter unit is also implemented in Flex5. The power controller is modelled in Matlab/Simulink. It calculates a power setpoint,  $P_{ref}$ , which is passed on to the generator-converter model in Flex5 (see Figure 2). The time traces of the grid frequency are processed with a low-pass (LP) filter with a cut-off frequency of 10 Hz. The cut-off frequency is set in accordance with the ENTSO-E recommendations [37]. The calculated power setpoint,  $P_{ref}$ , is limited by a maximum allowed power and a maximum allowed torque to protect the electrical and the mechanical part of the drive train. The maximum allowed power change for synthetic inertia,  $P_{SI}$ , is set to  $\pm 0.3$  pu. The simulation time step is 10 ms.

For the variable H controller, a demanded inertia constant,  $H_{dem}$ , has to be defined. In reality, this value would be defined by the transmission system operator. For the study at hand two different inertia constants are chosen, which have to be emulated by the WTG: 6 s, which allows a comparison to previously published results [34], and 12 s, which may be necessary to allow a stable grid operation in extreme situations (high shares of non-synchronous generation and large power imbalances [38,39]). In another previous study, 12 s has also been applied to maintain sufficient grid inertia in a turbulent part load wind [40].

The dynamic behavior of the WTG for the scenarios of the grid frequency as listed in Tables 1 and 2 is simulated in turbulent wind with a 0.17 turbulence intensity at 15 m/s wind speed. The simulated wind speeds are chosen such that an extrapolation to the full operating range of the WTG is possible. For the load calculation, the reactions of the WTG at different wind speeds are weighted based on a Weibull distribution to represent a site with an average wind speed of 7.3 m/s. In post-processing, these results are compared to the dynamic behavior without frequency support to calculate the load increases caused by the SI provision over the lifetime of the WTG (20 years). Hence,  $10^7$  load cycles are assumed. The analysis is carried out only for normal operation of the WTG (design load case 1.2 [31]).

The loads are analyzed for so-called sensors. Each sensor represents a one-directional torque or force at a certain segment of the WTG model. Hence, there are six sensors for each analyzed segment. Flex 5 uses different coordinate systems for the different segments of the WTG. An overview of the different coordinate systems used in Flex 5 is given in Sessarego et al. [41] For this analysis, the tower is represented by five segments (tower top, tower segment 1–3, and foundation), and the nacelle by three segments (main bearing, yaw bearing, and hub center). Furthermore, each blade root is analyzed individually. Hence, the loads are analyzed for 66 sensors in total.

The results of the time domain simulations and the load calculation are discussed in Sections 3.2 and 3.3, respectively.

### 3. Hardware-in-the-Loop and Simulation Results, Load Analysis, and Discussion

In the first part of this section, the results of the HiL tests are shown. This is followed by the time domain response of the WTG to exemplary frequency inputs, and finally the last section shows the results of the load calculations.

#### 3.1. Hardware-in-the-Loop Test Results and Discussions

The conducted HiL tests show the performance of a measurement system used in a real WT. To allow an easier comparison among grids with a different steady-state frequency, the frequencies and RoCoFs in Figures 8–10 are shown as normalized frequencies (base value 50 Hz). The varying time delay between the originally measured frequencies and those modelled in the HiL tests are caused by the HiL measurement setup and would not affect the mechanical loads of the WTG or the capability of the WTG to provide SI in a real grid.

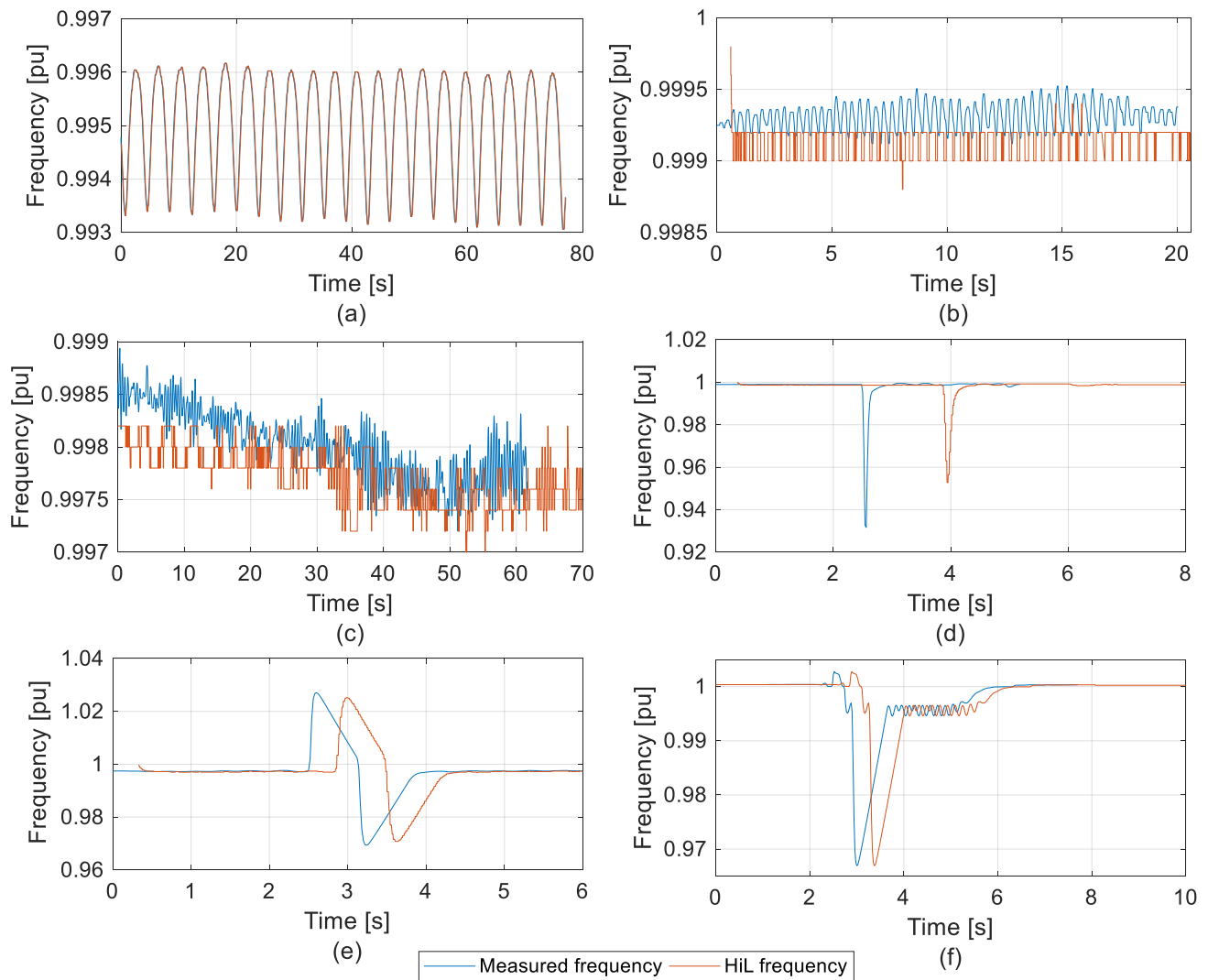


**Figure 8.** Comparison of the normalized measured frequency (blue) with the normalized frequency modelled in the hardware-in-the-loop test (orange) for scenario 1 (a), scenario 2 (b), scenario 4 (c), scenario 7 (d), scenario 8 (e), and scenario 10 (f).

The chosen time traces for the HiL tests allow a sufficient representation of the major characteristics of the frequency behavior for all scenarios defined in Section 2.1. The tests show that grid oscillations with a high frequency and small amplitudes cannot be measured reliably due to the limited accuracy of the measurement system. Hence, the simulation results for scenarios 2, 4 and 5 may differ from the reaction of a real WT (see Figure 8b,c). The time traces retrieved from the HiL tests are fundamentally different from the originally measured ones, especially when looking at the RoCoF (see Figure 9).

In contrast, slow oscillations with a higher amplitude occurred (see Figure 8a). Furthermore, high frequency oscillations can be measured if the amplitude is sufficiently high (see oscillations after the event in Figure 8f). Events can also be measured very well by the MFR (see Figure 8d–f). An exception is the nadir of frequency event for scenario 7, which is underestimated by approximately 2% (see Figure 8d). This may be caused by the short time the frequency stays in the nadir in combination with a very steep drop and rise, which may not be fully captured by the limited sampling time of the measurement system.

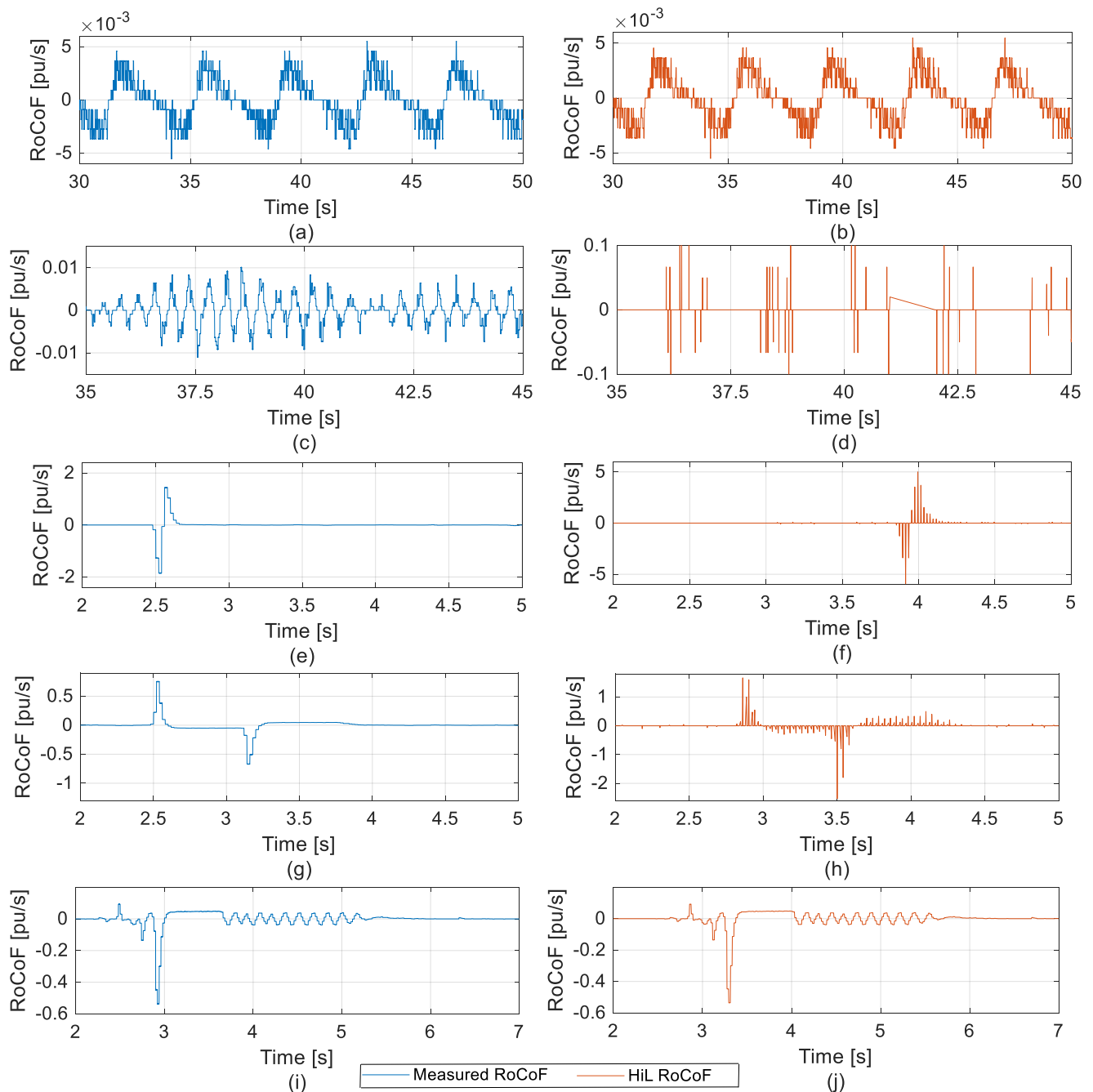


**Figure 9.** Comparison of the measured RoCoF (blue) with the RoCoF modelled in the hardware-in-the-loop test (orange) for parts of the time traces for scenario 1 (a,b), scenario 4 (c,d), scenario 7 (e,f), scenario 8 (g,h) and scenario 10 (i,j). Scenario 2 is shown in Figure 10.

For the IR of the WTG, the RoCoF is more important than the absolute value of the grid frequency (see Equation (1)). To allow an easier comparison between the original and the HiL signals, only parts of the scenario time traces are shown in Figure 9. When looking at the RoCoF, the limited sampling time of the measurement system in the HiL tests becomes also relevant for scenario 8 (see Figure 9g,h). As the MFR updates its output slower than the Bachmann controller reads its input, the RoCoF alternates between 0 Hz/s and very high RoCoF values (see Figure 9d,f,h). This effect is reduced by the LP filter used in the SI controller (see Figure 10). The slower and less extreme scenarios 1 and 10 are by contrast captured extremely well by the WTGs measurement system even when looking at the RoCoF (see Figure 9a,b,i,j).

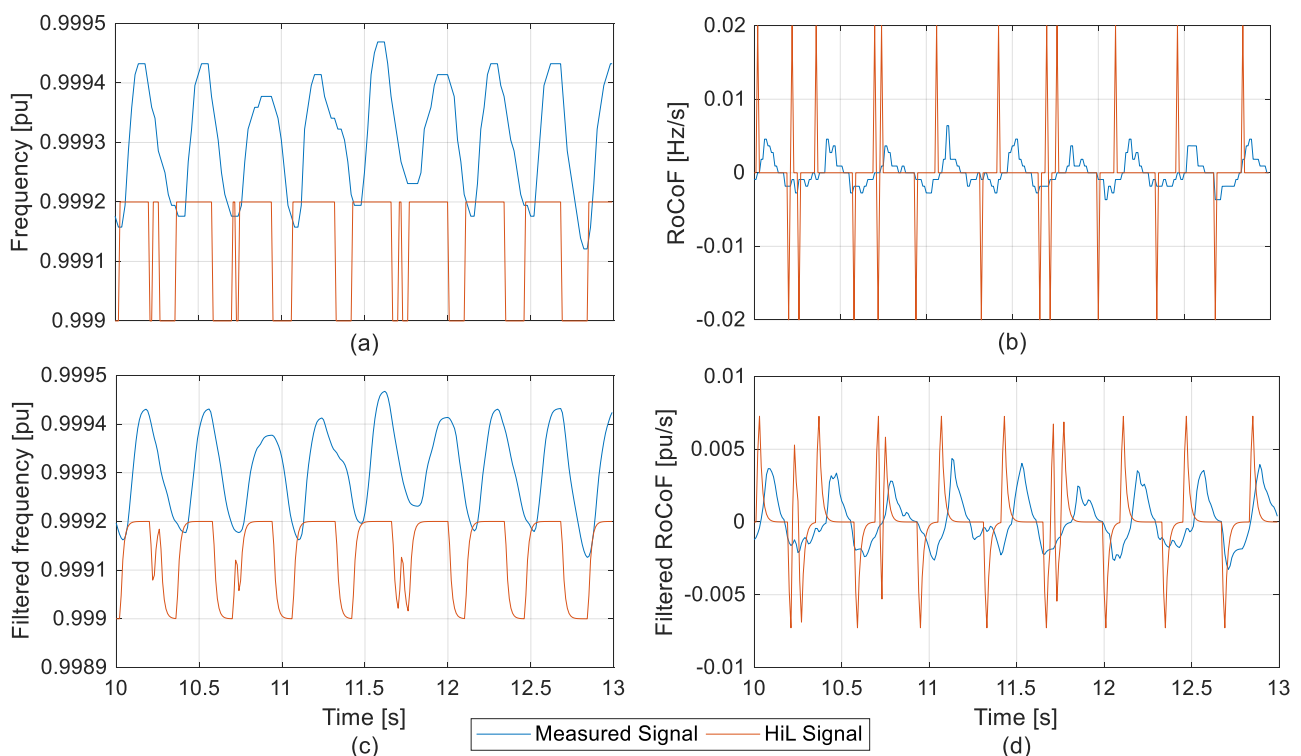


**Figure 10.** Comparison of the original frequencies and RoCoFs (blue) and HiL signals (orange) for a part of the time trace of scenario 2. (a) Shows the originally measured and the HiL frequency, (b) the corresponding RoCoFs to the signals in (a), (c) filtered version of the originally measured and the HiL frequency, and (d) the corresponding RoCoFs to the signals in (c). Time axes of (c,d) are valid for the above subplots as well.

The measured frequency signals are not used directly in the load simulations but are filtered with an LP filter with a cut-off frequency of 10 Hz (see Section 2.4). The RoCoF is calculated from these filtered signals. For the exemplary time traces of scenario 2, Figure 10 shows a comparison of the filtered measured and filtered HiL signals. Filtering the signals significantly decreases the RoCoF differences (see Figure 10b,d). The peaks of the HiL RoCoFs are reduced by a factor of 2.5 and are much closer to the peaks of the measured signals. However, the sinusoidal behavior of the signals is replaced by the LP filter response to the arbitrary jumps in the frequency (see Figure 10c,d).

For scenario 2 and 10, the WTG reaction to the HiL and the corresponding original time traces is shown and discussed in the next section. Furthermore, the acceleration of WTG components are compared for all scenarios, which are analyzed in the HiL tests.

### 3.2. Wind Turbine Simulations

In order to get an idea of the WTG reaction to the different frequency signals, time traces are shown and discussed for two exemplary scenarios. Furthermore, the differences between the measured frequency and the frequency generated in the HiL test is shown and discussed. Acceleration signals are analyzed for all scenarios for which HiL time traces are available. All simulations in this chapter are conducted with a demanded inertia constant,  $H_{dem} = 12$  s.

Figure 11 shows the reaction of the WTG to scenario 2, a fast oscillation of the grid frequency with a small amplitude (see Figure 10). The offset of the power setpoint,  $P_{SI}$  (see Figure 2), varies between  $\pm 0.06$  pu with a period of 0.37 s for the measured frequency signal (see blue line in Figure 11b). For the HiL frequency signal, the power setpoint varies almost arbitrarily between  $\pm 0.19$  pu (see red line in Figure 11b). This behavior is caused by the limitations of the measurement system as discussed in the previous section. However, a large part of the differences is reduced by the reaction of the generator-converter unit



to the setpoint changes. Hence, the differences in the generator power (see Figure 11c) are much smaller and for some parts of the time traces are almost negligible (e.g., 102 s to 106 s). As the WTG uses kinetic energy stored in the drive train to provide SI, the differences in the generator speed (see Figure 11d) follow the same pattern as the generator power. The generator speed oscillates almost sinusoidally as the physical inertia of the drive train dampens the sharper peaks of the generator power oscillations. The period of the oscillation resembles the period of the grid frequency variations. In the final seven seconds of the frequency oscillation, the WTG IR is occasionally limited by the maximum allowed drive train torque, thus limiting the generator power setpoint. Such limitations occurred for very short intervals: The longest duration of an ongoing limitation is 0.1 s. The total duration of all torque limitations in scenario 2 is 0.7 s (measured frequency signal) and 0.5 s (HiL signal). Such torque limitations also occur for other scenarios in high wind conditions and hamper the capability of the WTG to provide a reliable frequency support in high wind operating points.

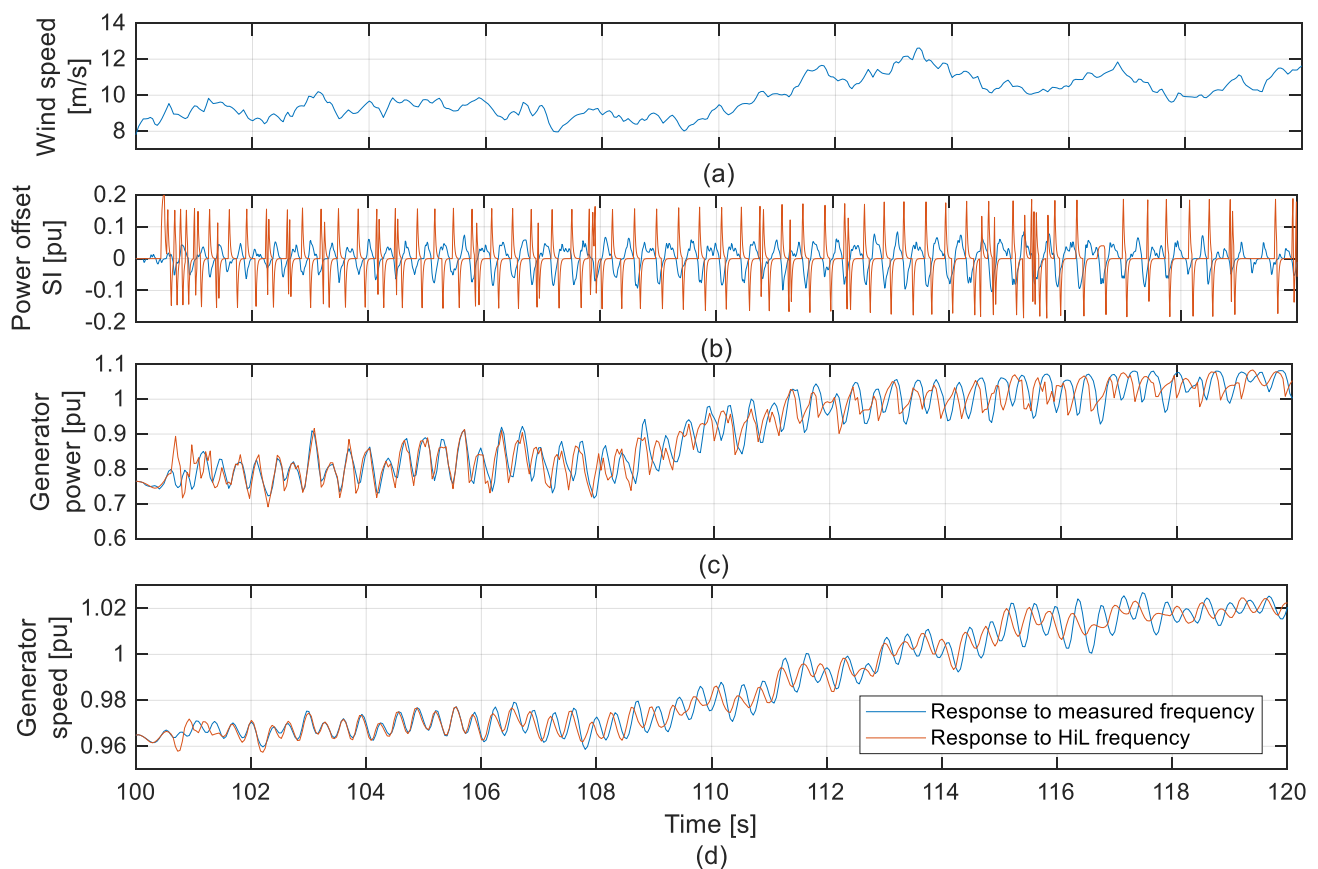


**Figure 11.** WTG reaction to scenario 2 for the measured frequency (blue) and the HiL frequency. (a) Wind speed, (b) power offset for SI provision, (c) generator power and (d) generator speed. Time axis of (d) is valid for the above subplots as well.

Figure 12 shows an example of the WTG's reaction to a severe frequency event. The IR is here often limited by the maximum allowed power offset for SI provision ( $\pm 0.3$  pu, see Figure 12b). The event and the following oscillation of the grid frequency causes drastic changes of the generator power, and consequently, of the generator speed (see Figure 12c,d). The different reactions of the WTG to the measured and the HiL frequency signal are mainly caused by the time delay of the HiL signal (appr. 0.4 s) and therefore slightly different wind conditions and operating points of the WTG. The grid frequency and the RoCoF for the two signals are almost identical (see Figures 8 and 9). Figure 12c,d also shows that the aerodynamic performance of the WTG is hardly affected by the drastic power changes, as the operating points of the WTG for both signals are almost identical

within one second after the last power offset for SI occurred. Furthermore, the results show the capability of the WTG to change its power output extremely fast: the maximum power gradient is close to  $\pm 4$  pu/s (see changes of generator power between 102.5 s and 104 s in Figure 12).

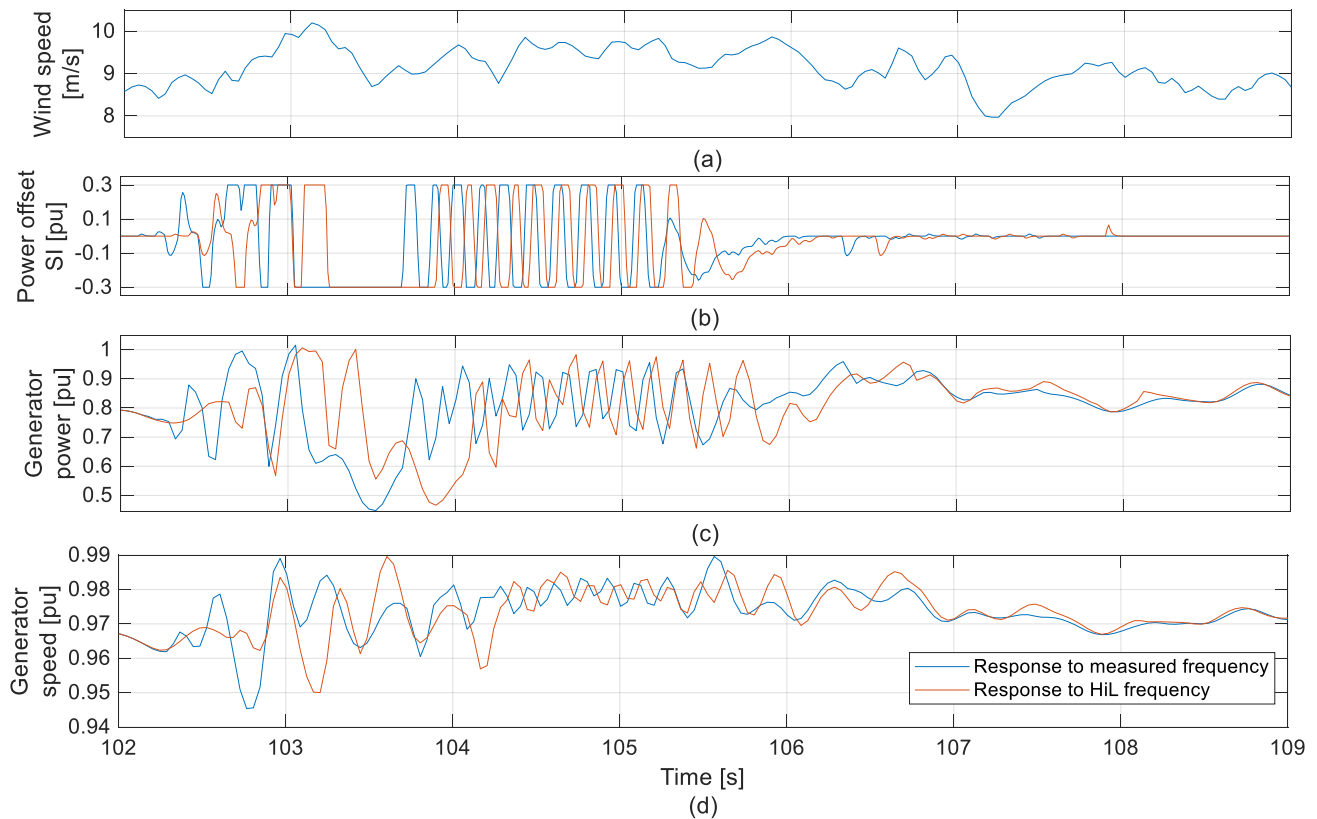


**Figure 12.** WTG reaction to scenario 10 for the measured frequency (blue) and the HiL frequency. (a) Wind speed, (b) power offset for SI provision, (c) generator power and (d) generator speed. Time axis of (d) is valid for the above subplots as well.

Such drastic changes of the applied electrical torque leads to heavy excitations of the drive train. Furthermore, drastic changes of the aerodynamic operating point may cause tower head motions. This may affect the lifetime of the WTG, which is discussed in detail in Chapter 3.3 for the measured frequency signals. In order to compare the HiL to the original frequency signals, the effect of IR on the WTG is estimated by comparing acceleration signals of the drive train and the tower head. The signals are chosen based on the results of a previous study [34]. The standard deviation of these signals is calculated for the original and the HiL scenarios and compared to the standard deviation during periods without SI provision in identical wind conditions.

Table 3 shows that the tower is much less affected than the drive train. In the for–aft direction, scenario 4 leads to the highest increase of the standard deviation for the originally measured signal. However, as scenario 4 represents a fast oscillation of the grid frequency, the effect is strongly reduced by the limitations of the WTG measurement system. When looking at the HiL frequency, the WTG is affected strongest in scenario 8. This scenario is characterized by a sharp increase in the frequency, followed by a longer decline and a longer rise of the frequency, which is well measurable in the HiL test (see Figure 8). Hence, the WTG shortly reduces its power, before it increases it for a longer time (approximately 0.7 s) and then reduces it again. This leads to a change of the WTG thrust, which causes a for–aft motion in the tower. For the side–side acceleration, the changes vary between 0.3% and 13%. Overall, the changes for the tower acceleration are small and can be neglected even for the extreme scenarios used in this study.

**Table 3.** Change of the standard deviation of the analyzed acceleration signals for six scenarios.

Scenario Number	Tower Head Acceleration (Fore—Aft)		Tower Head Acceleration (Side—Side)		Drive Train Acceleration	
	Measured Frequency	HiL Frequency	Measured Frequency	HiL Frequency	Measured Frequency	HiL Frequency
1	−6.7%	2.9%	2.9%	2.7%	3.5%	8.8%
2	3.2%	0.1%	1.7%	0.8%	133.6%	86.1%
4	18.1%	−0.2%	6.9%	0.3%	204.1%	57.2%
7	0.8%	3.6%	9.5%	13.0%	308.1%	222.4%
8	4.9%	−0.9%	5.7%	4.4%	202.7%	232.9%
10	2.5%	−0.7%	6.7%	6.7%	254.3%	253.2%

In contrast to the tower acceleration, the drive train acceleration is strongly affected by all scenarios apart from scenario 1 (slow oscillation of the grid frequency). In scenario 1, the power setpoint for SI varies slowly and with a smaller magnitude than the power variations arising from the turbulent wind. Hence, the drive train acceleration is only slightly increased. The fast oscillations of the grid frequency (scenarios 2 and 4) lead to a very high increase in the drive train accelerations. However, this increase is strongly reduced for the HiL time traces. The instantaneous peaks in the SI power offset (see Figure 11b, orange line and Figure 10) do not fully show in the generator power (see Figure 11c) as the generator-converter unit changes its operating point with some time delay. Hence, the drive train is less often excited and the speed becomes more stable. This behavior is strongest towards the end of scenario 2 (see Figure 11d). Grid frequency events (scenario 7, 8 and 10) strongly increase the drive train acceleration. For scenarios 8 and 10, there is no relevant difference between the measured and the HiL frequency. For scenario 7, there is a considerable reduction, but the increase remains at a high level. This is in line with the observation that grid frequency events can be captured very well by the WTG measurement system (see Figure 8). Hence, events, as well as fast oscillations, may strongly affect the WTG lifetime. The magnitude of this effect is quantified in the following section.

### 3.3. Load Analysis

The measurement and control system of each WTG differs and the analysis of the accelerations (see Table 3) shows that the measurement system is likely to reduce the loads of SI provision for the WTG. Hence, following a conservative approach, the originally measured frequencies are used in the load calculation. The loads are calculated for the SI provision case (i.e., for the scenarios listed in Tables 1 and 2). The resulting loads are compared to the loads without SI provision. The calculations are done for two demanded inertia constants: 6 s and 12 s.

For each sensor, the damage equivalent loads (DELs) of the frequency support case are divided by the damage equivalent loads of the reference case. These calculations are performed for various Woehler line exponents as these exponents are material depending (e.g., 4 is the relevant coefficient for steel towers while 10 is used for concrete towers). In addition, the load duration distribution (LDD) is calculated for the drive train to estimate the load increase for the rotating components (e.g., gearbox).

Table 4 shows the results of the load calculations. The data shows that the provision of SI has a negligible effect on the WTG loads. As expected, the highest increase is observed for the torsion in the drive train (sensor MzR1) due to the frequent changes of the generator torque. Furthermore, there are some smaller effects on the tower. There are no significant changes of the DELs for the blades. The increases for the LDD calculations of the drive train are also very small.

**Table 4.** Load changes for sensors with an increase of more than 0.1% caused by the provision of SI.

Sensor Name [41]	Sensor Description	Calculation Method	Woehler Coefficient	Load Increase, $H_{dem} = 6$ s	Load Increase, $H_{dem} = 12$ s
MzR1	Mainbearing torque	DEL	$m = 4$	0.21%	0.27%
MzR1	Mainbearing torque	DEL	$m = 8$	0.14%	0.65%
Mx	Tower top torsional moment	DEL	$m = 10$	0.12%	0.12%
My	Tower bottom fore–aft bending	DEL	$m = 4$	0.24%	0.20%
Mz	Tower bottom side–side bending	DEL	$m = 4$	0.17%	0.17%

There are various effects which explain the small increases of the loads, although extreme scenarios have been modelled. The requested power changes are typically very short and are often followed by another pulse in the opposite direction (increases/decreases). Hence, the generator-converter unit does not always reach the new operating point before an opposed signal starts. Therefore, the drive train speed changes little. Even for a longer power pulse, as in scenario 10, the drive train speed only oscillates with an amplitude of 0.02 pu (see Figure 12). Although frequency events occur regularly (2131 expected events per year, see Table 2), each event is only a few seconds long and hence the overall effect on the annual loads is small. Furthermore, the observed oscillations in the grid frequency (see Table 1) are not in the range of the eigenfrequency of the drive train. Hence, there are no resonance issues for the directly affected components of the WTG. This might be different for a different WTG or in a different grid, as the dominant oscillation frequencies are grid-specific [42]. During the simulations for scenario one, there were also no resonance issues for the tower. This can be partially explained by the aerodynamic damping through the wind speed changes for such a slow oscillation and partly by the shape of the time traces of the RoCoF, which only resemble a sinusoidal form (see Figure 9a,b).

There are also controller-related aspects, which explain the small effect on the WTG loads. The variable H controller was designed to make sure that the WTG provides more IR when the grid needs it and the WTG can provide it (i.e., high wind speeds and high instantaneous shares of inverter-based renewables [11]). Hence, during lower wind speeds, which occur regularly for onshore WTG, the WTG provides little IR and experiences and therefore there are also small changes in the loads. The load reduction by using a variable instead of a fixed inertia constant was shown in a previous study [34]. Furthermore, the torque limitation in the controller occasionally prevents an additional power supply by the WTG. While this has a positive effect on the WTG loads, it can be problematic for the grid when such a limitation occurs during a critical state of the grid. This problem is particularly important to overcome, as during high wind periods the grid is most likely to need SI provision from WTGs. During high wind periods, conventional power plants tend to shut down, especially when the high wind period lasts for a day or longer [43]. Hence, there is little conventional inertia in the grid causing a high demand for SI to stabilize the grid frequency. Therefore, WTGs should be able to supply SI reliably in these conditions. The full capability of the WTG to provide SI has to be ensured, e.g., by strengthening the drive train to allow higher torques. That may be achieved by replacing limiting components such as the coupling between the gearbox and the generator. A higher maximum torque is in return likely to increase the loading of the drive train. However, it is still expected to be in an order of magnitude, which does not make a complete redesign of the drive train necessary. The peaks in the demanded torque are directly related to calculation method for the RoCoF used in this study. It is chosen to create a worst-case, yet realistic scenario for the WTG. The effect of other methods or parameters on the magnitude of the RoCoF and consequently on the loads resulting from SI provision have not been studied. One critical parameter is the high cut-off frequency of the used LP filter. While this is backed by an ENTSO-E publication [37], the details of the RoCoF calculation still vary between different grid operators. Even in the cited document, different measuring time windows for the

RoCoF calculation are discussed. Any kind of averaging would result in smaller RoCoFs leading to smaller power offsets for SI provision and consequently to smaller maximum torque values. However, such an averaging would also lead to a delayed IR. Whether a faster or a slightly delayed but more robust response is favorable may depend on the particular grid in which SI is to be provided [44]. Hence, this topic is very critical: it may need to be discussed with the individual grid operator and will be investigated further in the future.

#### 4. Conclusions

The effect of SI provision on the loads of a state-of-the-art WTG is shown for comprehensive scenarios, which are based on the measurements of the Indian grid frequency. The detailed scenario definition allows a more realistic assessment of the dynamic excitations from SI provision and the resulting load increases than in previous studies. The study shows that supplying SI is marginally affecting the drive train. Other components of the WTG are de-facto unaffected. Hence, SI provision does not have to be prominently addressed in the load calculation of a WTG, although the RoCoFs of the analyzed grid abnormalities are very high and much larger than in previous studies [26–29]. The high RoCoFs are plausible as the Indian grid is considerably weaker than European grids and may therefore serve as an example for a future grid with higher shares of renewables, i.e., grids with little inertia. Furthermore, the RoCoF was calculated for short time intervals, which automatically leads to higher RoCoFs. However, the results are limited to the specific setup of the study as frequency analysis would differ for each grid (e.g., the frequency of inter-area-oscillations differ). This may lead to resonance problems if the eigenfrequencies of the WTG are close to the frequencies of the inter-area-oscillations. In addition, the results depend on the used controller and the design of the WTG. Furthermore, the measurement system of each WTG differs slightly, which would result in differences in the measured frequencies and differences in the SI provision of the WTG. Finally, the effect of an increased torque limitation on the loads is not considered in this study as it depends on the limitations of the new drive train components. However, the load increases are so small and the researched RoCoFs so high, that a different study setup is unlikely to change the results fundamentally.

In addition to the effects on the fatigue loads discussed in this study, SI provision may also lead to generator overspeed in extreme situations (e.g., system splits [39]). This problem may be overcome with a feedforward path to the speed controller. Such a control modification allows us to adapt the pitch angle faster and thus help to mitigate overspeeding due to SI provision. The exact design of the feedforward control is part of future research. Additionally, the effects of different RoCoF calculation methods and filter parameter on peaks of the electrical torque and the consequences for the SI provision will be studied in the future.

Considering all the limitations above, it is concluded that the continuous provision of SI can be achieved with a state-of-the-art WTG without significant effects on the lifetime of the WTG. This may help to stabilize future grids with little inertia.

**Author Contributions:** A.G.: conceptualization, methodology scenario definition, literature review, data analysis grid frequency, development of SI controller, visualization, writing—original draft preparation; C.J.: conceptualization, development of SI controller, discussions and comments, writing—review and editing; B.C.: conceptualization, methodology and conducting hardware in the loop tests; A.Z. implementation SI controller, conducting WTG simulations for load analysis, writing—review and editing J.W.: provision of data and resources, writing—review and editing. All authors have read and agreed to the published version of the manuscript.

**Funding:** This research is funded by the Bundesministerium für Bildung und Forschung und derand the gemeinsamen Wissenschaftskonferenz, project number 03IHS091. Parts of this paper are based on research funded by the Gesellschaft für Energie und Klimaschutz Schleswig-Holstein GmbH (EKSH), project number 8/12–20. The authors acknowledge financial support by the federal state of Schleswig-Holstein within the funding programme Open Access-Publikationsfonds.





EINE GEMEINSAME INITIATIVE VON

Bundesministerium  
für Bildung  
und ForschungGemeinsame  
Wissenschaftskonferenz  
GWK

**Institutional Review Board Statement:** Not applicable.

**Informed Consent Statement:** Not applicable.

**Data Availability Statement:** The data used in this study are confidential and are therefore not available to the public.

**Acknowledgments:** The authors thank Shubhangad Murkewar, Suzlon India, for his support with the load analysis and for his helpful insights during discussion of the results.

**Conflicts of Interest:** The authors declare no conflict of interest.

## References

1. EirGrid. EirGrid Grid Code. Version 9. December 2020. Available online: <https://www.eirgridgroup.com/site-files/library/EirGrid/GridCodeVersion9.pdf> (accessed on 15 January 2021).
2. Hydro-Québec TransÉnergie. Technical Requirements for the Connection of Generating Stations to the Hydro-Québec Transmission System. D-2018-145, January 2019. Available online: [http://www.hydroquebec.com/transenergie/fr/commerce/pdf/2\\_Requirements\\_generating\\_stations\\_D-2018-145\\_2018-11-15.pdf](http://www.hydroquebec.com/transenergie/fr/commerce/pdf/2_Requirements_generating_stations_D-2018-145_2018-11-15.pdf) (accessed on 15 January 2021).
3. Central Electricity Authority. Technical Standards for Connectivity to the Grid (Amendment). 2019. Available online: [https://cea.nic.in/wp-content/uploads/2020/02/notified\\_regulations.pdf](https://cea.nic.in/wp-content/uploads/2020/02/notified_regulations.pdf) (accessed on 15 January 2021).
4. O’Sullivan, J.; Rogers, A.; Flynn, D.; Smith, P.; Mullane, A.; O’Malley, M. Studying the Maximum Instantaneous Non-Synchronous Generation in an Island System—Frequency Stability Challenges in Ireland. *IEEE Trans. Power Syst.* **2014**, *29*, 2943–2951. [CrossRef]
5. Yu, M.; Roscoe, A.J.; Dysko, A.; Booth, C.; Ierna, R.; Zhu, J.; Urdal, H. Instantaneous penetration level limits of non-synchronous devices in the British power system. *IET Renew. Power Gener.* **2017**, *11*, 1211–1217. [CrossRef]
6. Chown, G.; Wright, J.; van Heerden, R.; Coker, M. System inertia and Rate of Change of Frequency (RoCoF) with increasing non-synchronous renewable energy penetration. In Proceedings of the 8th Southern Africa Regional Conference, Cape Town, South Africa, 14–17 November 2017.
7. Díaz-González, F.; Hau, M.; Sumper, A.; Gomis-Bellmunt, O. Participation of wind power plants in system frequency control: Review of grid code requirements and control methods. *Renew. Sustain. Energy Rev.* **2014**, *34*, 551–564. [CrossRef]
8. Eriksson, R.; Modig, N.; Elkington, K. Synthetic inertia versus fast frequency response: A definition. *IET Renew. Power Gener.* **2017**, *12*, 507–514. [CrossRef]
9. Godin, P.; Fischer, M.; Roettgers, H.; Mendonca, A.; Engelken, S. Wind power plant level testing of inertial response with optimised recovery behaviour. *IET Renew. Power Gener.* **2019**, *13*, 676–683. [CrossRef]
10. Ramtharan, G.; Jenkins, N.; Ekanayake, J.B. Frequency support from doubly fed induction generator wind turbines. *IET Renew. Power Gener.* **2007**, *1*, 3. [CrossRef]
11. Gloe, A.; Jauch, C.; Craciun, B.; Winkelmann, J. Limitations for the continuous provision of synthetic inertia with wind turbines. In Proceedings of the 16th Wind Integration Workshop, Berlin, Germany, 25–27 October 2017; pp. 442–447.
12. Manwell, J.F.; McGowan, J.G.; Rogers, A.L. *Wind Energy Explained: Theory, Design and Application*, 2nd ed.; Wiley: Chichester, UK, 2011.
13. Hansen, M.O. *Aerodynamics of Wind Turbines*, 3rd ed.; Routledge: London, UK, 2015. [CrossRef]
14. Hau, E. *Wind Turbines: Fundamentals, Technologies, Application, Economics*, 3rd ed.; Springer: Berlin, Germany, 2013.
15. Fleming, P.A.; Van Wingerden, J.-W.; Scholbrock, A.K.; Van Der Veen, G.; Wright, A.D. Field testing a wind turbine drive-train/tower damper using advanced design and validation techniques. In Proceedings of the 2013 American Control Conference, Washington, DC, USA, 17–19 June 2013; pp. 2227–2234. [CrossRef]
16. Rahim, N.A.; Khyam, M.O.; Li, X.; Pesch, D. Sensor Fusion and State Estimation of IoT Enabled Wind Energy Conversion System. *Sensors* **2019**, *19*, 1566. [CrossRef]
17. Ritter, B.; Schild, A.; Feldt, M.; Konigorski, U. The design of nonlinear observers for wind turbine dynamic state and parameter estimation. *J. Phys. Conf. Ser.* **2016**, *753*, 052029. [CrossRef]
18. Saenz-Aguirre, A.; Zulueta, E.; Fernandez-Gamiz, U.; Ulazia, A.; Teso-Fz-Betoño, D. Performance enhancement of the artificial neural network-based reinforcement learning for wind turbine yaw control. *Wind. Energy* **2019**, *23*, 676–690. [CrossRef]
19. Jie, W.; Jingchun, C.; Lin, Y.; Wenliang, W.; Jian, D. Pitch control of wind turbine based on deep neural network. *IOP Conf. Ser. Earth Environ. Sci.* **2020**, *619*, 012034. [CrossRef]



20. Schlipf, D. *Lidar-Assisted Control Concepts for Wind Turbines*; University of Stuttgart: Stuttgart, Germany, 2016. [CrossRef]
21. Gaur, S.; Elias, S.; Höbbel, T.; Matsagar, V.; Thiele, K. Tuned mass dampers in wind response control of wind turbine with soil-structure interaction. *Soil Dyn. Earthq. Eng.* **2020**, *132*, 106071. [CrossRef]
22. Jauch, C. Grid Services and Stress Reduction with a Flywheel in the Rotor of a Wind Turbine. *Energies* **2021**, *14*, 2556. [CrossRef]
23. Joos, G. Wind turbine generator low voltage ride through requirements and solutions. In Proceedings of the 2008 IEEE Power and Energy Society General Meeting—Conversion and Delivery of Electrical Energy in the 21st Century, Pittsburgh, PA, USA, 20–24 July 2008; pp. 1–7. Available online: <http://ieeexplore.ieee.org/document/4596605/> (accessed on 10 February 2021).
24. Wenske, J.; Beckert, U. Voltage-induced stresses during Low-Voltage Ride Through (LVRT) in the drive train of wind turbines with DFIG. *Renew. Energy Power Qual. J.* **2012**, *1*, 1094–1099. [CrossRef]
25. Arbeiter, M.; Hopp, M.; Huhn, M. LVRT Impact on Tower Loads, Drivetrain Torque and Rotational Speed—Measurement Results of a 2-MW Class DFIG Wind Turbine. *Energies* **2021**, *14*, 3539. [CrossRef]
26. Fleming, P.A.; Aho, J.; Buckspan, A.; Ela, E.; Zhang, Y.; Gevorgian, V.; Scholbrock, A.; Pao, L.; Damiani, R. Effects of power reserve control on wind turbine structural loading. *Wind. Energy* **2015**, *19*, 453–469. [CrossRef]
27. Wang, X.; Gao, W.; Scholbrock, A.; Muljadi, E.; Gevorgian, V.; Wang, J.; Yan, W.; Zhang, H. Evaluation of different inertial control methods for variable-speed wind turbines simulated by fatigue, aerodynamic, structures and turbulence (FAST). *IET Renew. Power Gener.* **2017**, *11*, 1534–1544. [CrossRef]
28. Fischer, B.; Shan, M.; Brosche, P.; Loepelmann, P.; Rezaeian, A.; Sayed, M.; Hauptmann, S. Abschlussbericht GridLoads, Kassel, Stuttgart, Technical Report. 2020. Available online: [https://www.mesh-engineering.de/images/Publications/MesH/Abschlussbericht\\_GridLoads\\_final.pdf](https://www.mesh-engineering.de/images/Publications/MesH/Abschlussbericht_GridLoads_final.pdf) (accessed on 17 March 2021).
29. Fischer, B.; Duckwitz, D.; Shan, M.; Sayed, M.; Rezaeian, A. On Interactions of Drive Trains in Wind Farms Providing Power System Inertia. In Proceedings of the Wind Energy Science Conference, Cork, Ireland, 17–20 June 2019. Available online: [https://www.researchgate.net/publication/334030049\\_On\\_interactions\\_of\\_drive\\_trains\\_in\\_wind\\_farms\\_providing\\_power\\_system\\_inertia](https://www.researchgate.net/publication/334030049_On_interactions_of_drive_trains_in_wind_farms_providing_power_system_inertia) (accessed on 17 March 2021).
30. Øye, S. FLEX4, Simulation of Wind Turbine Dynamics. In *State of the Art of Aerolastic Codes for Wind Turbine Calculations*; Pedersen, B.M., Ed.; Technical University of Denmark: Lyngby, Denmark, 1996; pp. 71–76.
31. International Electrotechnical Commission. *IEC 61400-1, Wind Energy Generation Systems—Part 1: Design Requirements*; International Electrotechnical Commission: Geneva, Switzerland, 2019.
32. Gloe, A.; Jauch, C.; Craciun, B.; Winkelmann, J. Continuous provision of synthetic inertia with wind turbines: Implications for the wind turbine and for the grid. *IET Renew. Power Gener.* **2019**, *13*, 668–675. [CrossRef]
33. International Electrotechnical Commission. *IEC 61400-21, Wind Energy Generation Systems—Part 21: Measurement and Assessment of Power Quality Characteristics of Grid Connected Wind Turbines*; International Electrotechnical Commission: Geneva, Switzerland, 2008.
34. Gloe, A.; Jauch, C.; Thiesen, H.; Viebeg, J. *Inertial Response Controller Design for a Variable Speed Wind Turbine*; Technical Report; Wind Energy Technology Institute: Flensburg, Germany, 2018.
35. Typhoon HIL. Typhoon HIL602, Product Brochure. Available online: <https://www.typhoon-hil.com/doc/products/Typhoon-HIL602-brochure.pdf> (accessed on 1 July 2021).
36. Bachmann Electronic. ‘System Overview’, Product Brochure. 2019. Available online: [https://www.bachmann.info/uploads/tx\\_sbdowloader/systemoverview\\_11\\_2019\\_en.pdf](https://www.bachmann.info/uploads/tx_sbdowloader/systemoverview_11_2019_en.pdf) (accessed on 1 July 2021).
37. ENTSO-E. ‘Frequency Measurement Requirements and Usage’, Final Version 7. 2018. Available online: [https://eepublicdownloads.entsoe.eu/clean-documents/SOC%20documents/Regional\\_Groups\\_Continental\\_Europe/2018/TF\\_Freq\\_Meas\\_v7.pdf](https://eepublicdownloads.entsoe.eu/clean-documents/SOC%20documents/Regional_Groups_Continental_Europe/2018/TF_Freq_Meas_v7.pdf) (accessed on 19 March 2021).
38. Fernández-Guillamón, A.; Gómez-Lázaro, E.; Molina-García, Á. Extensive frequency response and inertia analysis under high renewable energy source integration scenarios: Application to the European interconnected power system. *IET Renew. Power Gener.* **2020**, *14*, 2885–2896. [CrossRef]
39. Gloe, A.; Jauch, C.; Räther, T. Grid Support with Wind Turbines: The Case of the 2019 Blackout in Flensburg. *Energies* **2021**, *14*, 1697. [CrossRef]
40. Jauch, C.; Gloe, A. Simultaneous Inertia Contribution and Optimal Grid Utilization with Wind Turbines. *Energies* **2019**, *12*, 3013. [CrossRef]
41. Sessarego, M.; Ramos-García, N.; Sørensen, J.N.; Shen, W.Z. Development of an aeroelastic code based on three-dimensional viscous-inviscid method for wind turbine computations. *Wind. Energy* **2017**, *20*, 1145–1170. [CrossRef]
42. Domínguez-García, J.L.; Gomis-Bellmunt, O.; Bianchi, F.D.; Sumper, A. Power oscillation damping supported by wind power: A review. *Renew. Sustain. Energy Rev.* **2012**, *16*, 4994–5006. [CrossRef]
43. Matevosyan, J.; Anderson, C.; Li, W. ERCOT Future Synchronous Inertia Projections. In Proceedings of the 16th Wind Integration Workshop, Berlin, Germany, 25–27 October 2017.
44. Miller, N.; Pajic, S. Diverse fast frequency response services in systems with declining synchronous inertia. In Proceedings of the 15th Wind Integration Workshop, Vienna, Austria, 15–17 November 2016.